

# The scintillation method

## 1 Introduction

When electromagnetic (EM) radiation propagates through the atmosphere it is distorted by a number of processes that can influence its characteristics, e.g., its intensity (or amplitude), polarization and phase. Two of these processes are scattering and absorption by constituent gasses and atmospheric particles of the atmosphere, which remove energy from the beam and thus lead to attenuation. Note that by far the most important characteristic of scattered radiation is its intensity. The most serious mechanism that influences the propagation of EM radiation is small fluctuations in the refractive index of air ( $n$ ). These turbulent refractive index fluctuations in the atmosphere lead e.g., to intensity fluctuations and are also known as scintillations. Some examples that clearly show the distortion of wave propagation by the turbulent atmosphere, which can be seen regularly, are the twinkling of stars, image dancing and image blurring above a hot surface.

In most cases the atmosphere behaves turbulent. Turbulence is described as three-dimensional air motions or eddies, which have sizes ranging between millimetres to tens of metres. Turbulence in the atmosphere is the most effective transport mechanism for many scalar quantities, such as heat and water vapour. The refractive index of air is a function of the temperature ( $T$ ) and to a lesser degree the humidity ( $Q$ ) of the air, i.e., the density of the air ( $\rho$ ). As eddies transport both heat and water vapour their refractive indices are different from their surroundings, resulting in refractive index fluctuations and thus scintillations.

Since the 1950s many scientists have conducted theoretical studies trying to explain scintillation phenomena. Several different theoretical approaches have been proposed to describe the propagation of EM radiation in a turbulent medium. In some approaches the turbulent eddies are visualized as a collection of positive and negative lenses, which focus or defocus the beam resulting in scintillations. In others diffractive effects are taken into account. In the 1960s with the invention of the laser, experimental studies were conducted to validate the proposed propagation models. It was found that some of these models were very successful in describing certain phenomena for certain regimes.

Due to the success of the models that were able to relate the propagation statistics of EM radiation with the turbulent properties of the atmosphere, it is now possible to measure and quantify the turbulent characteristics of the atmosphere using a remote sensing method, also known as the scintillation method. A scintillometer is an instrument that consists of a light source (transmitter part) and a detector (receiver part) that measures intensity fluctuations. Because the measured variance of intensity fluctuations is a measure of the turbulent behaviour of the atmosphere it can indirectly be related to the transport of certain quantities. Depending on the configuration of the scintillometer, e.g. the aperture size, wavelength and the number of receivers the fluxes of heat, water vapour and momentum can be derived.

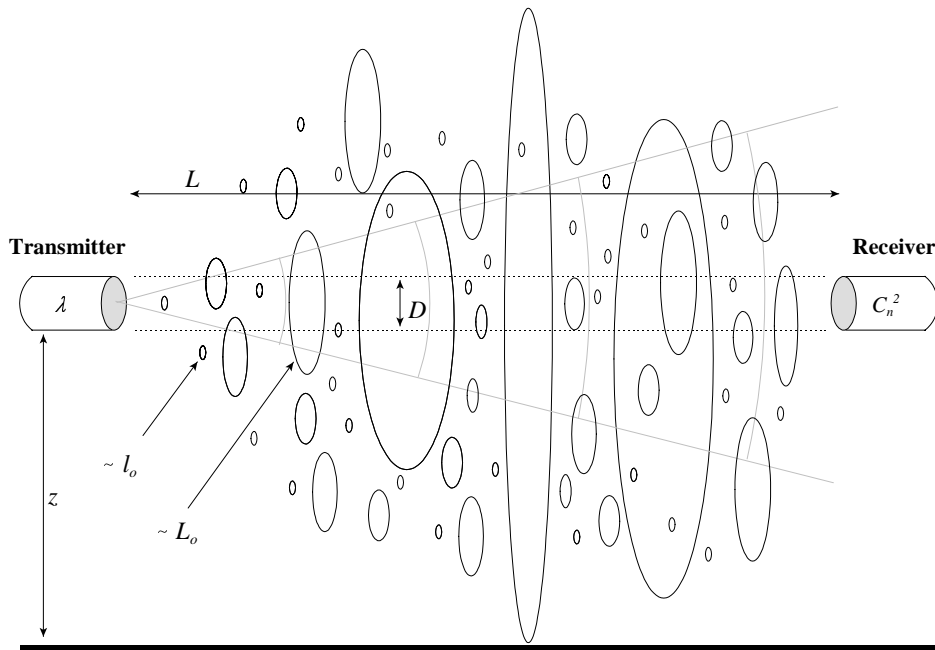


**Figure 1: Schematic of a scintillometer set-up where the EM beam emitted by the transmitter is scattered by turbulent eddies in the atmosphere. Also some important length scales are shown.**

A schematic of a scintillometer set-up is shown in Figure 1. The transmitter emits a beam of light with a certain wavelength ( $\lambda$ ). At a known distance  $L$  from the light source the receiver analyses the intensity fluctuations (expressed as  $C_n^2$ ) that are caused by the turbulent eddies. Also a number of length scales are shown that play a role in scintillometry; the diameter of the beam ( $D$ ), the different eddy sizes bounded by  $l_o$  and  $L_o$  and the height of the scintillometer above the surface ( $z$ ).

In the next paragraphs the basics of the scintillation method will be explained. As reference the papers selected by Andreas (1990) and the comprehensive review paper by Moene (2002) were used. The turbulent spectrum of refractive index fluctuations will be discussed in Paragraph 2. Structure functions, which are used to describe the behaviour of EM waves in random media, are explained in Paragraph 3. Several different wave propagation models have been proposed to describe the propagation of EM radiation in a turbulent medium. In Paragraph 4 the approaches and limitations of some of them are discussed briefly. The most successful approach that links the propagation statistics of EM radiation with the turbulent characteristics of the atmosphere is given in Paragraph 5. An important limitation of the scintillation method, known as saturation, is discussed in Paragraph 6. By increasing the aperture size of the scintillometer the path length can be extended without saturation effects. The basics of aperture averaging and the large aperture scintillometer (LAS) are explained in Paragraph 7. Both temperature and humidity fluctuations are responsible for fluctuations in the refractive index of air. This means that the measured  $C_n^2$  can be related to  $C_T^2$  and  $C_Q^2$ . Paragraph 8 will show that the contribution of temperature and humidity fluctuations is wavelength dependant. In Paragraph 9 is explained how the fluxes of heat ( $H$ ) and latent heat ( $L_v E$ ) can be derived from  $C_T^2$  and  $C_Q^2$  using the Monin-Obukhov similarity theory. Finally, Paragraph 10 gives a short summary of the scintillation method.

## 2 The turbulent spectrum

In the atmospheric boundary layer (ABL) the flow behaves generally very chaotic, i.e., turbulent. Turbulence consists of a wide range of three-dimensional whorls, usually called eddies. In general the largest eddies are generated by both wind shear and convection (dependant on local climatology) and have a size in the order of the boundary layer depth. The large scale eddies are unstable and brake down into smaller and smaller eddies, known as the cascade process. Finally, the turbulent kinetic energy ( $\varepsilon$ ) is dissipated into heat at the smallest molecular length scales, called the Kolmogorov micro scale

$$\eta = \left( \frac{\nu^3}{\varepsilon} \right)^{\frac{1}{4}}. \quad (2.1)$$

With typical values for the viscosity of air ( $\nu$ ) and the molecular dissipation rate of turbulent kinetic energy ( $\varepsilon$ ),  $\eta$  is in the order of 1 mm.

In Figure 2 a representation of the energy spectrum is depicted, which shows the distribution of the turbulent kinetic energy with wave number ( $\kappa$ ). The wave number is defined as  $\kappa = 2\pi/l$ , where  $l$  is the size of the eddy. At eddy scales larger than the outer scale  $L_o$  ( $K_o = 2\pi/L_o$ ) energy is introduced in the turbulent spectrum. In this part of the spectrum turbulence is not isotropic and inhomogeneous. In general the size of the outer scale is in the order of half the height above the surface ( $z$ ). At wave number higher than  $K_m$ , which is related to the inner scale  $l_o$  ( $K_m = 2\pi/l_o$ ), the turbulent kinetic energy is dissipated into heat. Typical size of the inner scale is 1 mm to 10 mm. Hill and Clifford (1978) defined the inner sale as the intersection point of the asymptotic forms of the structure functions (see Paragraph 3) in the inertial and dissipation ranges. They showed that the inner scale is related to the Kolmogorov micro scale as follows

$$l_o = 7.4 \left( \frac{\nu^3}{\varepsilon} \right)^{\frac{1}{4}}. \quad (2.2)$$

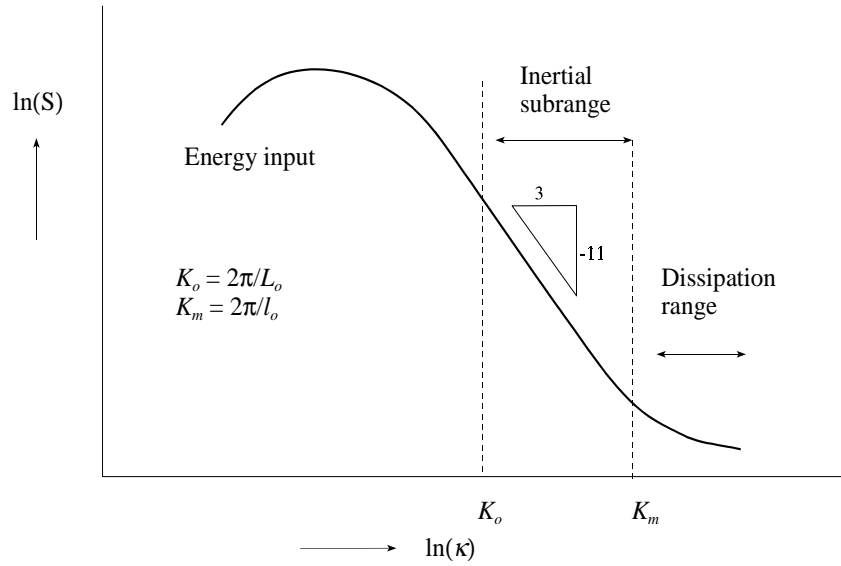


**Figure 2: Schematic representation of the energy spectrum of turbulence.**

Part of the spectrum, which lies between the inner scale and outer scale of turbulence, is called the inertial sub range. This part of the spectrum is independent of the energy input and the viscous dissipation and where only the inertial transfer of energy is important. In the cascade process from large to intermediate and small size eddies Kolmogorov hypothesized that these small eddies have no memory of the large-scale processes and turbulence becomes isotropic at the high wave numbers (Garraat, 1992).

Based on the concept of the cascade process Kolmogorov proposed the following form for the three-dimensional spectrum of refractive index fluctuations ( $\Phi_K(\kappa)$ ) in the atmosphere (Tatarskii, 1961)

$$\Phi_K(\kappa) = 0.033 C_n^2 \kappa^{-\frac{11}{3}}, \quad (2.3)$$

where  $\kappa$  is the wave number and  $C_n^2$  is the structure parameter of the refractive index of air (see Paragraph 2.3). This model is only valid for the inertial sub range, although it is often extended over all wave numbers by assuming the inner scale is zero and the outer scale is infinite. However, it was found that the model overestimates  $\Phi_K(\kappa)$  in the dissipation range (i.e. it falls off more rapidly than  $-11/3$ ). Therefore, Tatarskii (1961) proposed the following model

$$\Phi_T(\kappa) = 0.033 C_n^2 \kappa^{-\frac{11}{3}} \exp\left(\frac{-\kappa^2}{\kappa_m^2}\right), \quad (2.4)$$

where  $\kappa_m = 5.92/l_o$ . This model uses a Gaussian cut-off at high spatial wave numbers, which results in a steeper falloff than  $\kappa^{-11/3}$ . This can be seen in Figure 3 where both the Kolmogorov ( $\Phi_K(\kappa)$ ) and Tatarskii ( $\Phi_T(\kappa)$ ) spectral model are shown.

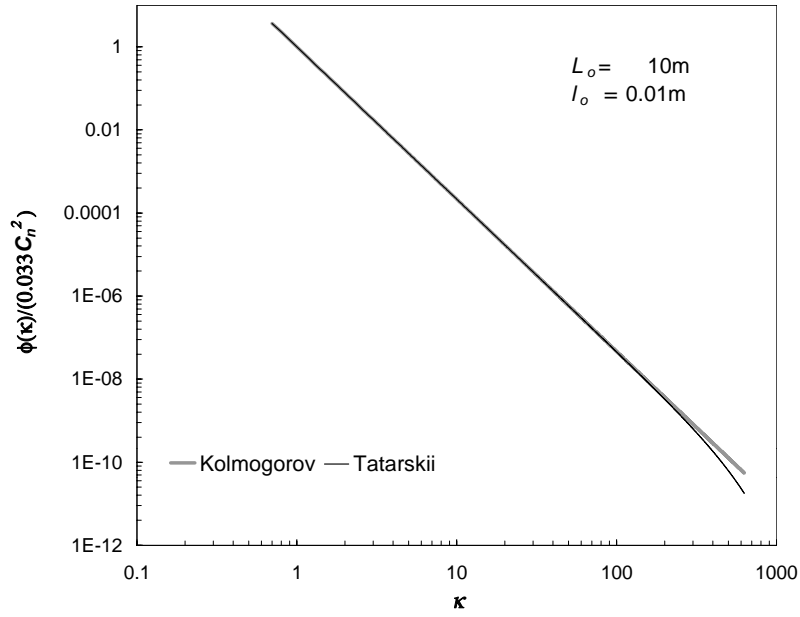


**Figure 3: Spectral models by Kolmogorov ( $\Phi_K(\kappa)$ ) and Tatarskii ( $\Phi_T(\kappa)$ ) of refractive index fluctuations.**

Fast temperature and velocity measurements by Champagne et al. (1977) and Williams and Paulson (1977) revealed a 'bump' in the spectrum at high wave numbers near  $l_o^{-1}$ . Neither the model of Kolmogorov nor that of Tatarskii exhibits this bump. Based on the data of Champagne et al. (1977) Hill (1978) developed a theoretical model ( $\Phi_H(\kappa)$ ) that describes this bump and agrees well with the observations. Churnside (1990) derived an analytical approximation to the Hill model

$$\Phi_C(\kappa) = 0.033C_n^2 \kappa^{-11/3} \left[ \exp\left(-70.5\kappa^2 \left(\frac{l_o}{7.5}\right)^2\right) + 1.45 \exp\left(-0.97 \left(\ln\left(\kappa \frac{l_o}{7.5}\right) + 1.55\right)^2\right) \right]. \quad (2.5)$$

Frehlich (1992) determined  $\Phi_F(\kappa)$  directly from laser scintillation measurements. In Figure 4 the Hill-spectrum (1978) is shown together with the models of Churnside (1990) and Frehlich (1992). It can be seen that model of Tatarskii shows no bump and the models of Churnside and Frehlich slightly differ from the Hill spectrum. In Paragraph 5 will be shown that the exact form of the spectrum  $\Phi(\kappa)$  at high wave numbers is important to know, especially when a near infrared point source/detector scintillometer is used (see e.g., Hartogensis et al, 2002a; De Bruin and Meijninger, 2002). The reason is that these scintillometer types are most sensitive to eddy sizes in the order of the inner scale  $l_o$ , i.e. close to the bump in the spectrum. On the other hand a large aperture scintillometer is most sensitive to eddy sizes in the order of the aperture diameter ( $D$ ) and is therefore less sensitive to the bump and thus the exact form of  $\Phi(\kappa)$ .

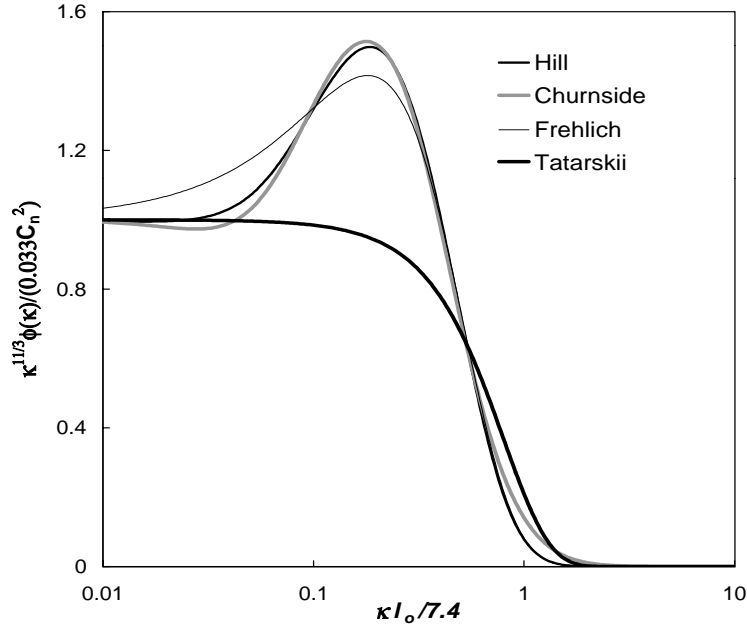


Figure 4: Scaled spectral models of refractive index fluctuations of Hill (1978), Churnside (1990) and Frehlich (1992) showing the ‘Hill’ bump plotted together with the Tatarskii spectrum as a function of the wave number scaled by the inner scale ( $l_0/7.4$ ).

### 3 The structure parameter of the refractive index of air $C_n^2$

Wind speed ( $u$ ), air temperature ( $T$ ), the refractive index ( $n$ ) and other quantities undergo irregular random fluctuations in a turbulent atmosphere. Random processes in space and time can be described by random functions, e.g.,  $n(t)$ , which is a random function describing the refractive index of air. However random functions are difficult to determine. In practice one uses statistical characteristics of the random functions. An important characteristic of a random function is the correlation function  $B(\mathbf{r}_1, \mathbf{r}_2)$ , which describes the spatial structure of turbulence. The correlation function describing the refractive index fluctuations in a random field  $n(\mathbf{r})$  is as follows (Tatarskii, 1961)

$$B_n(\mathbf{r}_1, \mathbf{r}_2) = \langle [n(\mathbf{r}_1) - \langle n(\mathbf{r}_1) \rangle] [n'(\mathbf{r}_2) - \langle n'(\mathbf{r}_2) \rangle] \rangle, \quad (2.6)$$

where a random field can be considered as a random function of three variables (e.g. the three velocity components in a velocity field) and the angle brackets denote an ensemble average.  $B_n$  describes the mutual relation between the fluctuations of a scalar  $n$  at different locations in space ( $\mathbf{r}_1$  and  $\mathbf{r}_2$ ). A random field is statistically homogeneous if it has a constant mean and  $B_n$  is unaffected by a simultaneous translation of  $\mathbf{r}_1$  and  $\mathbf{r}_2$  in the same direction by the same amount, i.e.

$$\langle n(\mathbf{r}) \rangle = \text{const}, \quad B_n(\mathbf{r}_1, \mathbf{r}_2) = B_n(\mathbf{r}_1 + \mathbf{r}_0, \mathbf{r}_2 + \mathbf{r}_0). \quad (2.7)$$

Choosing  $\mathbf{r}_0 = -\mathbf{r}_2$ , the correlation function in a homogeneous field depends only on the difference  $\mathbf{r}_1 - \mathbf{r}_2$

$$B_n(\mathbf{r}_1, \mathbf{r}_2) = B_n(\mathbf{r}_1 - \mathbf{r}_2, 0) = B_n(\mathbf{r}_1 - \mathbf{r}_2). \quad (2.8)$$

A homogeneous random field is isotropic if  $B_n$  only depends on  $r = |\mathbf{r}|$ , i.e. only on the distance between the points and not the direction

$$B_n(\mathbf{r}_1, \mathbf{r}_2) = B_n(r). \quad (2.9)$$

However homogeneous and isotropic random fields are only crude approximations to real meteorological fields. For example, most statistical characteristics of atmospheric turbulence are a function of altitude. Therefore, as with non-stationary random processes, it is better to use structure functions instead of correlation functions.

The difference of the field values  $n(\mathbf{r})$  between  $\mathbf{r}_1$  and  $\mathbf{r}_2$  is mainly influenced by those inhomogeneities of the field  $n$ , which are smaller than  $|\mathbf{r}_1 - \mathbf{r}_2|$ . If this distance is not too large, the largest inhomogeneities have no effect on  $n(\mathbf{r}_1) - n(\mathbf{r}_2)$  and therefore the (second order) structure function

$$D_n(\mathbf{r}_1, \mathbf{r}_2) = \left\langle \left[ (n(\mathbf{r}_1) - \langle n(\mathbf{r}_1) \rangle) - (n(\mathbf{r}_2) - \langle n(\mathbf{r}_2) \rangle) \right]^2 \right\rangle, \quad (2.10)$$

depends on  $\mathbf{r}_1 - \mathbf{r}_2$  only. This hypothesis, proposed by Kolmogorov, is known as local homogeneity. Thus the value of  $D_n$  characterizes the intensity of those fluctuations of  $n$  with scales smaller than or equal to  $\mathbf{r}_1 - \mathbf{r}_2$ . On the other hand  $B_n(\mathbf{r}_1, \mathbf{r}_2)$  depends not only on the distance  $\mathbf{r}_1 - \mathbf{r}_2$  but also on  $\mathbf{r}_1$  and  $\mathbf{r}_2$  separately and therefore depends on inhomogeneities of all scales.

In case of a locally homogeneous random field ( $\langle n(\mathbf{r}) \rangle = \text{const}$ ), the structure function only depends on  $\mathbf{r}_1 - \mathbf{r}_2$

$$D_n(\mathbf{r}_1, \mathbf{r}_2) = D_n(\mathbf{r}_1 - \mathbf{r}_2). \quad (2.11)$$

Finally, a locally homogenous random field is locally isotropic if  $D_n$  only depends on  $|\mathbf{r}_1 - \mathbf{r}_2|$ , i.e. only on the distance and not the direction, which leads to the following simplified form of the structure function

$$D_n(\mathbf{r}) = D_n(r) = \left\langle [n(\mathbf{r}'+\mathbf{r}) - n(\mathbf{r}')]^2 \right\rangle. \quad (2.12)$$

The structure function is related to the three-dimensional spectrum as follows (Tatarskii, 1961)

$$D_n(r) = 8\pi \int_0^{\infty} \left(1 - \frac{\sin \kappa r}{\kappa r}\right) \Phi(\kappa) \kappa^2 d\kappa. \quad (2.13)$$

By inserting only the inertial sub range part of the spectrum the following well-known relationship for a locally isotropic field can be derived

$$D_n(r) = C_n^2 r^{2/3}, \quad l_o \ll r \ll L_o \quad (2.14)$$

where  $C_n^2$  is the structure parameter of the refractive index of air. When turbulence is homogeneous and isotropic within the inertial sub range  $C_n^2$  is independent of  $r$  and is a measure of the amount of turbulent refractive index fluctuations. A larger value corresponds with more turbulent mixing of air.

## 4 Wave propagation theory in random media

When an EM wave propagates through a turbulent medium (e.g., the atmosphere) it suffers from scattering mechanisms and absorption. The most important mechanism that causes scattering in the atmosphere is random fluctuations in the refractive index of air. Both Obukhov and Tatarskii were one of the first who did theoretical studies on scintillation phenomena based on wave equations. Later on followed by experimental studies using lasers. So far the theory of optical propagation of EM waves through random media is not fully understood, except for certain regimes.

Several theoretical models have been developed that describe certain phenomena of line-of-sight wave propagation in a random medium (Lawrence and Strohbehn, 1970; Strohbehn, 1969; Tatarskii, 1961). One of these is the geometrical optics approach (Tatarskii, 1961; 1971). In this approach amplitude fluctuations are attributed to the focusing and defocusing of the EM rays by the curvature of the turbulent eddies along the path, i.e. the eddies are considered as a collection of positive and negative lenses. This approach has been successfully applied to the line-of-sight propagation of short wavelengths, i.e. wavelengths that are small compared to the inner scale of turbulence ( $\lambda \ll l_o$ ). *This is mainly needed to ensure that small-angle scattering can be assumed* (Strohbehn, 1968). Tatarskii (1961; 1971) showed that in the geometrical optics method the smallest inhomogeneities of the order of  $l_o$  are the most essential for intensity fluctuations (small eddies are more curved than large ones). The main restriction of the geometrical optics method is that it ignores diffractive spreading. Diffractive spreading, which has a scale size of  $F = \sqrt{\lambda L}$  also known as the first Fresnel zone, can be seen around the shadow of a certain object at a screen. In case the object is much larger than the scale of diffractive spreading, diffraction effects can be ignored ( $F \ll l_o$ ). Because  $F$  depends on the propagation distance  $L$  a certain point will be reached where  $F$  will become larger. When this happens the focusing and defocusing process by lenses of the order of  $l_o$  no longer contribute to the observed intensity fluctuations, instead

diffractional effects become dominant. Because  $F$  depends on  $L$  the geometrical optics method is restricted to short path lengths (see Paragraph 6).

An alternative approach is the method of smooth perturbations, which takes diffraction effects into account (Tatarskii, 1961; 1971). As a result this approach is valid over longer distances. However, the method assumes that the wave is only perturbed slightly from its original state (i.e. weak scattering), which in practise again limits the distance.

The best method so far is the so-called Rytov method, which is also a perturbation method and accounts for diffractional effects. Originally it was claimed that it would overcome the latter limitation of the smooth perturbation method. Later, experimental studies proved otherwise. The main difference between the two perturbation methods is that the Rytov method is applied to a transformation of the wave equation used in the original perturbation approach. Nevertheless, a perturbation method is only valid when the perturbations are small (i.e. weak turbulence conditions) and thus restricts the propagation distance.

The starting point of all methods is the wave equation, which represents the propagation of a monochromatic wave through a random medium thereby neglecting polarisation effects (Lawrence and Strohbehn, 1970; Andrews et al., 2001)

$$\nabla^2 E(r) + k^2 n^2(r) E(r) = 0. \quad (2.15)$$

$\nabla^2$  is the three-dimensional Laplacian operator of an electromagnetic wave  $E$ ,  $k$  the optical wave number ( $= 2\pi/\lambda$ ) and  $n$  the refractive index of the medium. The first term includes diffraction effects, which are ignored in the geometrical optics method.

In the atmosphere it is known that the refractive index fluctuations around its mean value are very small. Based on this fact a perturbation expansion is used in order to solve Equation 2.15. I.e. a perturbation expansion of  $E$  and  $n$ ;  $E = E_0 + E_1$  where  $E_0$  is the incident electric field and  $E_1$  the scattered field and  $n = 1 + n_1$  where  $n_1 \ll 1$ . It must be noted that in the perturbation expansion only the first scattering term is considered (i.e.  $E_2, E_3 \dots = 0$ ) in order to derive an analytical solution. In Paragraph 6 experimental evidence will reveal that ignoring these higher-order terms restricts the validity of derived solutions of Equation 2.15. In the Rytov method the wave equation is transformed by substituting  $\Psi = \ln(E)$ . Considering a plane wave  $E = Ae^{iS}$ , where  $A$  is the amplitude and  $S$  the phase,  $\Psi$  becomes

$$\Psi = \chi + iS. \quad (2.16)$$

If the perturbations are small, i.e.  $E_1 \ll E_0$ , a solution of Equation 2.15 can be derived in the form of an unperturbed and perturbed part, where the amplitude ( $\chi$ ) and phase ( $S'$ ) fluctuations can be expressed as

$$\chi = \ln\left(\frac{A}{A_0}\right) \quad (2.17)$$

and

$$S' = S - S_0, \quad (2.18)$$

where  $A_0$  and  $S_0$  are the amplitude and phase of the unperturbed wave  $E_0$ . A similar perturbation approach is applied to Equation 2.15 for spherical waves (i.e., a point source/detector). In the next Paragraph the solution of the Rytov method for spherical waves will be discussed, which is applicable for small aperture scintillometers.

## 5 Statistical solution of the wave equation

The solution of the wave equation following the Rytov approach for spherical waves (i.e. point source/detector) propagating through a random medium, which is statistically homogeneous and locally isotropic, is as follows (Lawrence and Strohbehn, 1974)

$$\sigma_\chi^2 = 4\pi^2 k^2 \int_0^L dx \int_0^\infty d\kappa \kappa \Phi(\kappa) \sin^2\left(\frac{\kappa^2 x(L-x)}{2kL}\right). \quad (2.19)$$

$\sigma_\chi^2$  is the variance of the logarithm of amplitude fluctuations ( $\chi$ ) measured by a small aperture scintillometer (SAS),  $k$  the optical wave number,  $L$  the path length,  $\kappa$  the (spatial) wave number and  $\Phi(\kappa)$  the three-dimensional spectrum of refractive index fluctuations. Inserting the Kolmogorov spectrum thereby ignoring small-scale effects and carrying out the integration gives the following relation between  $\sigma_\chi^2$  and the path averaged  $C_n^2$  (Tatarskii, 1961)

$$\sigma_\chi^2 = 0.124 k^{\frac{7}{6}} L^{\frac{11}{6}} C_n^2, \quad l_o \ll F \ll L_o, \sigma_\chi^2 < 0.3. \quad (2.20)$$

This equation, which is based on the first-order scattering theory, is only valid in the weak scattering regime and is therefore only applicable when  $\sigma_\chi^2 < 0.3$  (Clifford et al., 1974, Paragraph 6). Small scale effects can be ignored when  $F \gg l_o$ . For example a scintillometer that operates at a radio wavelength of 11 mm has a Fresnel size of several meters, thus  $F \gg l_o$ . When the wavelength lies in the visible to near-infrared wavelength region  $F$  approximately equals  $l_o$ . In that case small effects cannot be ignored and an accurate three-dimensional spectrum (i.e. the Hill spectrum) must be substituted instead, which leads to the following expression

$$\sigma_{\chi}^2 = 0.124k^{\frac{7}{6}}L^{\frac{11}{6}}C_n^2\Phi\left(\frac{l_o}{F}\right), \quad l_o \approx F \ll L_o, \sigma_{\chi}^2 < 0.3, \quad (2.21)$$

where the function  $\Phi(l_o/F)$  accounts for the small scale effects. Important to note is that due to the large Fresnel zone of a scintillometer that operates at a wavelength of 11 mm the scintillometer becomes more sensitive to outer scale effects because  $F$  approaches  $L_o$ . Note that Equations 2.20 and 2.21 are often expressed as a function of intensity fluctuations ( $\sigma_{\text{int}}^2 = 4\sigma_{\text{int}A}^2 = 4\sigma_{\chi}^2$ ) because most scintillometers measure intensity fluctuations.

When Equation 2.19 is written in a more convenient form, showing the averaging of  $C_n^2$  along the path  $L$

$$\sigma_{\chi}^2 = \int_0^L C_n^2(x)W(x)dx \quad (2.22)$$

the path weighting function  $W(x)$  can be derived

$$W(x) = 4\pi^2k^2 \int_0^{\infty} d\kappa \kappa \Phi(\kappa) \sin^2\left(\frac{\kappa^2 x(L-x)}{2kL}\right) \approx \left(\frac{x}{L}\left(1 - \frac{x}{L}\right)\right)^{5/6}. \quad (2.23)$$

An example of the path weighting function is depicted in Figure 5 (assuming the detector approximates a point detector), which shows that the path weighting function has its maximum in the centre of the path and gradually drops to zero at the ends. This means that the scintillometer is most sensitive to 'scintillating' eddies in the middle of its path.

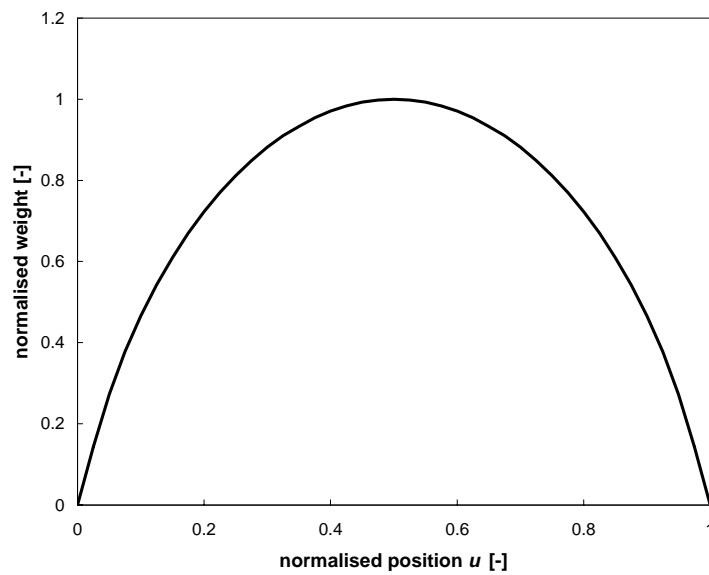


**Figure 5: The path weighting function ( $W$ ) of a point source transmitter/detector (i.e. a spherical wave) as a function of the relative position  $u$  ( $= x/L$ ).**

In order to analyse the size of the eddies that produce the most powerful scintillations the integrand of Equation 2.23, rewritten as

$$\kappa\Phi(\kappa)\sin^2\left(\frac{\kappa^2\frac{x}{L}\left(1-\frac{x}{L}\right)F^2}{4\pi}\right), \quad (2.24)$$

has to be analysed. For  $x/L = 0.5$  and  $0.05$  this integrand is plotted in Figure 6 as a function of  $F/l$  ( $= F\kappa/2\pi$ ). The Figure reveals that the optically most effective eddies are of the order of the diameter of the first Fresnel zone  $F$  in the centre of the path ( $x/L = 0.5$ ) and decreases in size towards the transmitter and receiver ends ( $x/L = 0.05$ ). As mentioned before, depending on the configuration of the scintillometer (i.e.  $\lambda$ ) and its set-up (i.e.  $L$ )  $F$  varies between several millimetres to a few meters.

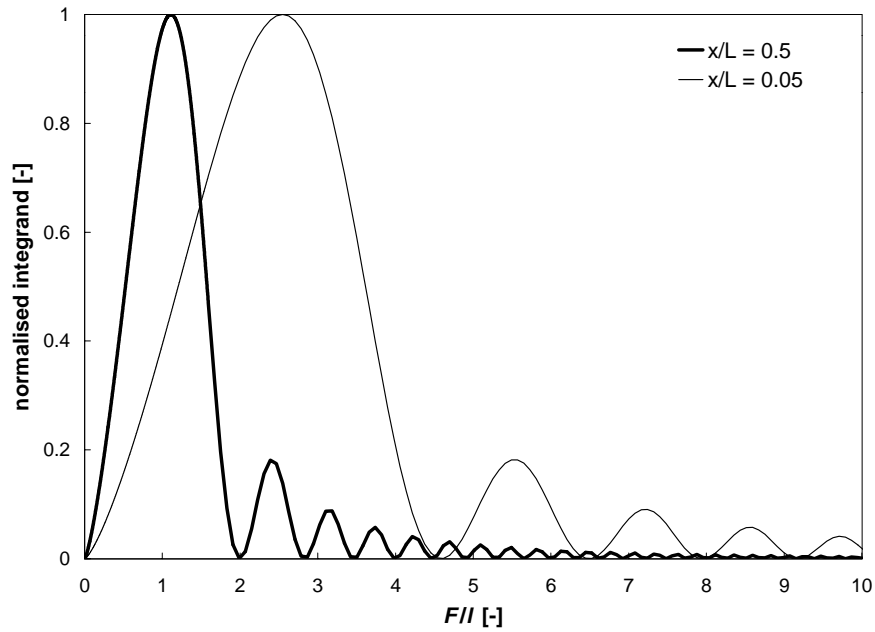


**Figure 6: Values of the integrand (normalized to 1) as a function of the size of the inhomogeneity  $l$ , which is normalized by the first Fresnel zone  $F$  (for  $x/L = 0.5$  and  $0.05$ ).**

A more simple physical model to derive the size of the optically most effective eddies is shown in Figure 7 (Clifford et al., 1974). This Figure shows an irregularity (e.g., an eddy) of diameter  $2l$  at an arbitrary point X between the transmitter (S) and the receiver (at distance L). The eddy will be most effective in producing a 'scintillation' at point L when the difference between path SAL and SL equals  $\lambda/2$ , i.e. in this way the two rays interfere destructively. Note that it is assumed that the spherical wave is scattered only once. Working out the geometry gives

$$l \approx \sqrt{\pi \left( \frac{x}{L} \right) \left( 1 - \frac{x}{L} \right)} \sqrt{\lambda L}. \quad (2.25)$$

Again the most optically eddy has a size of approximately  $F$  in the centre ( $x/L = 0.5$ ) and decreases in size towards the ends ( $x/L \rightarrow 0$  and  $1$ ). If there are smaller eddies than  $F$  at point X scintillations will be produced at places, which lie between point X and the receiver (L). Although these scintillations eventually will reach point L their contribution to the total variance at the receiver is small. On the other hand eddy sizes larger than  $F$  will not produce

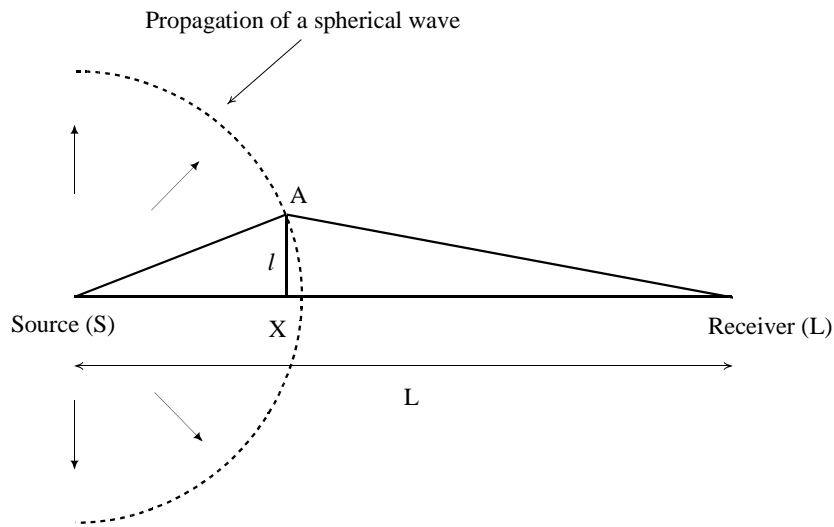


**Figure 7: The geometry of a simple eddy model. The receiver (L) observes scintillations of a spherical wave emitted by the transmitter (S), which are produced by an eddy/irregularity at point X.**

## 6 Saturation

Equation 2.19 is based on first-order scattering theory (i.e., the wave is scattered only once, see Paragraph 4). Therefore, this Equation is only valid in a weak scattering medium. If the turbulence becomes too intense (i.e. a strong scattering medium where scattering occurs more than once) the proportionality between  $\sigma_\chi^2$  and  $C_n^2$  will fail. This phenomenon is known as saturation of the signal. Clifford et al. (1974) found that saturation occurs when  $\sigma_\chi^2 > 0.3$ . When this happens a further increases of  $C_n^2$  no longer result in an increase of  $\sigma_\chi^2$ . Figure 8 shows observed values of  $\sigma_\chi^2$  plotted against theoretical predicted values of  $\sigma_\chi^2$  using Equation 2.19 and known values of  $k$  and  $L$  and  $C_n^2$  values derived from temperature probes. It can be seen that for all path lengths except the shortest saturation occurs. Over extreme long path lengths a point will be reached where  $\sigma_\chi^2$  starts to decrease. This is called super saturation (see Figure 8 for  $L = 1750$  m).

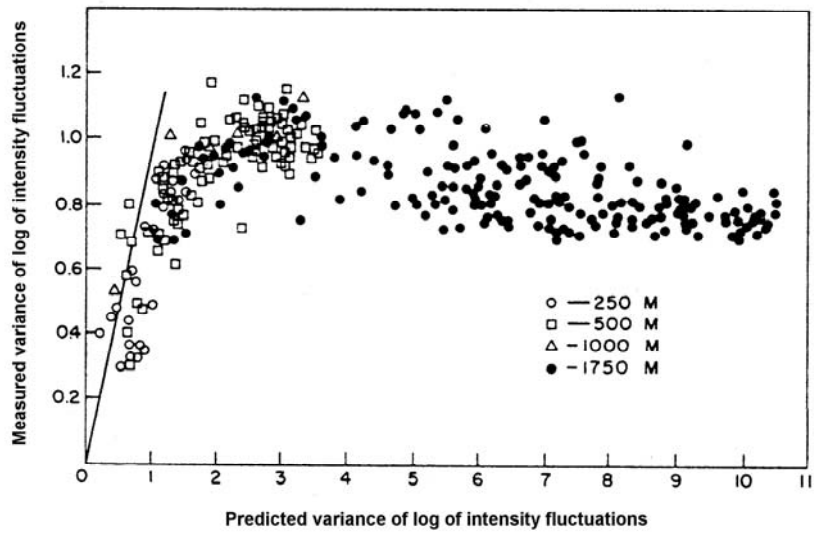


**Figure 8: Measured values of  $\sigma_{\chi}^2$  (vertical axis) plotted against modelled  $\sigma_{\chi}^2$  values (horizontal axis) showing the saturation effect which occurs over long path lengths (Strohbehn, 1968). The solid line equals a 1:1 line.**

Clifford et al. (1974) explained the saturation effect as follows, which is sketched in Figure 9. As the wave passes through a strong scattering medium lenses at both sides of the lens  $F$  will be distort the wave front resulting in small irregularities in the wave front. When the size of these irregularities is smaller than the size of  $F$  the power of lens  $F$  will be diminished. Finally, this results in a pattern at  $x = L$ , which is different in size compared with the pattern for a single scattering situation with an undisturbed spherical wave front. This effect is known as smearing of the pattern and will result in a decrease of  $\sigma_{\chi}^2$ . When the size of lens  $F$  becomes smaller and smaller eventually a point will be reached where there can be no irregularities in the wave front than the smallest eddy  $l_o$ . This means that if lens  $F$  has the size  $l_o$  it can no longer be distorted and is effective in producing scintillations. In the case the irregularities in the wave front are larger than the  $F$  the pattern at point  $x = L$  will not change in size but only its position will shift on the screen (this can be seen as tilting of the wave front). To summarize over longer path lengths the most effective eddies are no longer of the scale size of the first Fresnel zone. Instead smaller scales become dominant. According to the turbulent power spectrum small scale turbulence is less powerful than large scale turbulence resulting in a decrease of  $\sigma_{\chi}^2$  as is shown in Figure 8.

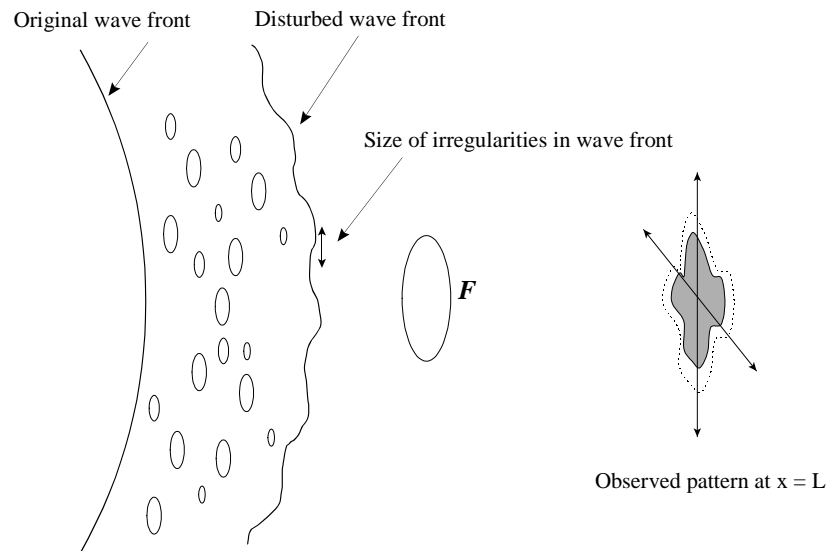


**Figure 9: Schematic representation of the smearing effect caused by irregularities smaller than lens  $F$  under strong turbulent conditions.**

## 7 The Large Aperture Scintillometer

A simple way to avoid saturation is by limiting the path length. Another way to overcome saturation of the signal is to increase the aperture size ( $D$ ) of the scintillometer (Wang et al., 1978). When the aperture size of the receiver is larger than the scale of the optically most effective eddies ( $F$ ) the receiver will average out fluctuations of the received signal over the aperture area. This process, called aperture averaging leads to reduced intensity fluctuations.

In Figure 10 a schematic of the averaging effect is shown. Due to the diffraction process in the atmosphere a scintillation pattern, which consists of a wide range of dark and bright structures, will drift over a screen positioned at the receiver side. A very small receiver will be sensitive to all these scales in the scintillation pattern. As the aperture of the receiver increases fine scale structures in the pattern will average out over the aperture, i.e., small dark and bright spots will compensate. As a result  $\sigma_{\chi}^2$  will decrease. Very large-scale structures in the scintillation pattern, which are larger than the aperture diameter, will not be seen because they don't produce intensity fluctuations. On the other hand structures that are in the order of the aperture diameter will be dominant. Although it is less apparent, the same averaging occurs when the diameter of the transmitter increases (assuming an incoherent source). In this case the aperture of the transmitter can be regarded as a collection of point sources, which filter out fine scale turbulence.

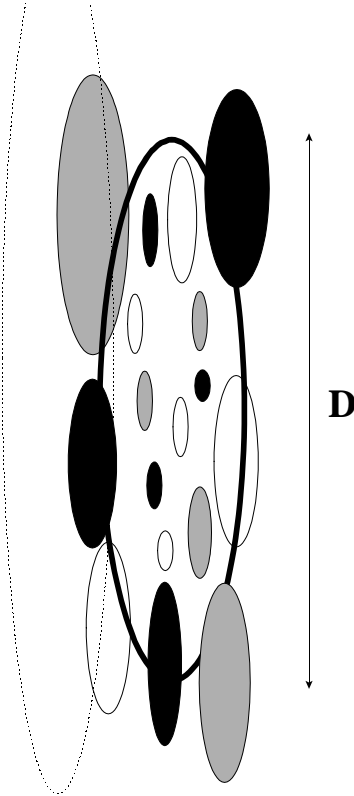


**Figure 10: Schematic of aperture averaging of fine scale turbulence.**

For equal transmitting and receiving apertures with diameter  $D$ , the expression for  $\sigma_\chi^2$  is as follows (Hill and Ochs, 1978)

$$\sigma_\chi^2 = 4\pi^2 k^2 \int_0^L dx \int_0^\infty d\kappa \kappa \Phi(\kappa) \sin^2\left(\frac{\kappa^2 x(L-x)}{2kL}\right) \cdot \left[ \left( \frac{2J_1\left(0.5\kappa D \frac{x}{L}\right)}{0.5\kappa D \frac{x}{L}} \right) \cdot \left( \frac{2J_1\left(0.5\kappa D \left(1 - \frac{x}{L}\right)\right)}{0.5\kappa D \left(1 - \frac{x}{L}\right)} \right) \right]^2, \quad (2.26)$$

where  $J_1$  is the Bessel function. Note that this expression is still based on the first-order scattering theory, which means that a large aperture scintillometer also has saturation point. The term between the brackets accounts for the aperture averaging. For infinite small aperture (i.e.  $D \rightarrow 0$ ) this term approaches unity and the resulting equation is valid again for a point source/detector scintillometer (Equation 2.19). In Figure 11 this term is plotted as a function of wave number. At high wave numbers this term goes to zero, i.e., small-scale turbulence is filtered out.

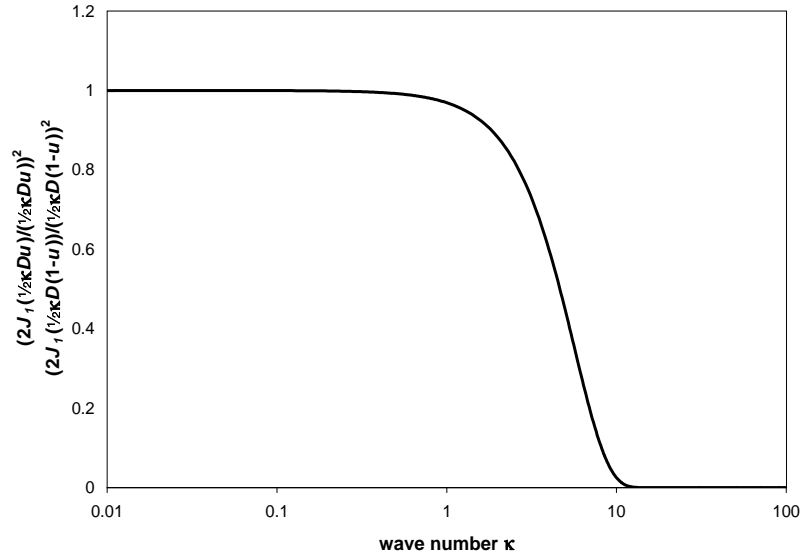


**Figure 11: The ‘aperture averaging’ term of Equation 2.26 as a function of wave number (for  $u = 0.5$ ).**

After inserting the spectrum of refractive index fluctuations and integrating Equation 2.26 the relation between  $\sigma_\chi^2$  and the path averaged  $C_n^2$  for a large aperture scintillometer can be derived (Wang et al., 1978)

$$\sigma_\chi^2 = 0.223 D^{-3} L^3 \overline{C_n^2}, \quad l_o \ll F \ll D \ll L_o. \quad (2.27)$$

Important to note is that aperture size must be sufficiently large. In Figure 12 the normalized variance  $\sigma_\chi^2$  is plotted as a function of the normalized aperture diameter  $\alpha (= D/F)$ . It can be seen that  $\sigma_\chi^2$  is only proportional to  $\alpha^{-7/3}$  when  $\alpha$  is larger than 2, i.e.,  $D > 2F$ . This means that if  $L$  becomes too large Equation 2.27 is no longer valid.

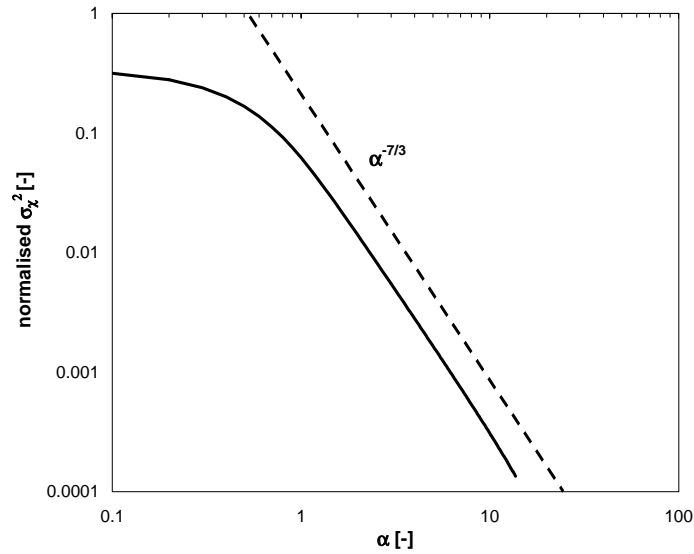


**Figure 12: The normalized  $\sigma_\chi^2$  as a function of  $\alpha (= D/F)$ . For small  $\alpha$  (i.e., small  $D$ )  $\sigma_\chi^2$  is no longer proportional to  $\alpha^{-7/3}$ .**

As for the point source/detector scintillometer Equation 2.26 can be re-written in a more convenient form to derive the path weighting function  $W(x)$  for a LAS

$$W(x) = 4\pi^2 k^2 \int_0^\infty d\kappa \kappa \Phi(\kappa) \sin^2\left(\frac{\kappa^2 x(L-x)}{2kL}\right) \cdot \left[ \left( \frac{2J_1\left(0.5\kappa D \frac{x}{L}\right)}{0.5\kappa D \frac{x}{L}} \right) \cdot \left( \frac{2J_1\left(0.5\kappa D \left(1-\frac{x}{L}\right)\right)}{0.5\kappa D \left(1-\frac{x}{L}\right)} \right) \right]^2. \quad (2.28)$$

The path weighting function is depicted in Figure 13, which shows that a large aperture scintillometer is also most sensitive in the centre of its path.

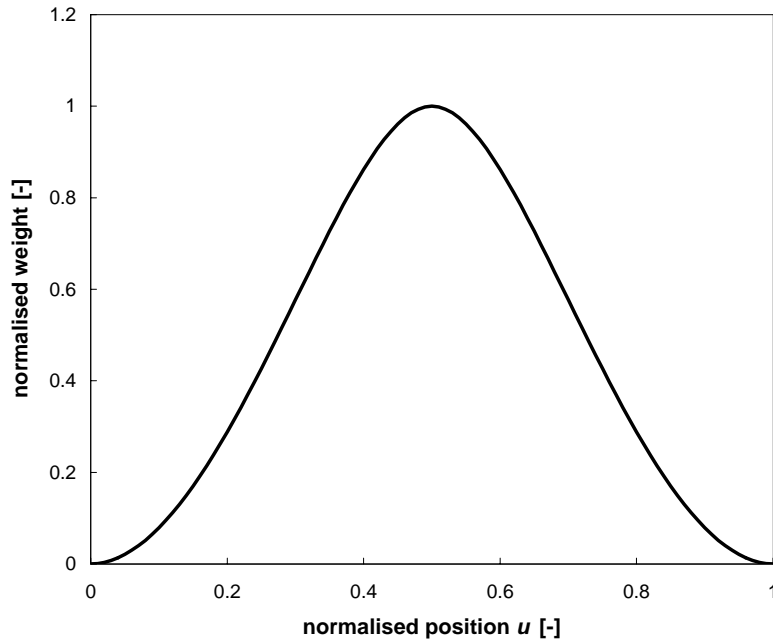


**Figure 13: The path weighting function ( $W$ ) of a large aperture scintillometer ( $\lambda = 940 \text{ nm}$ ) as a function of the relative position  $u$  ( $= x/L$ ).**

In Figure 14 the integrand of Equation 2.28 is shown. This Figure is similar to Figure 6 showing the most effective eddy seen by a scintillometer. In Figure 14 the peak of the integrand lies at a scale of the order of the aperture diameter  $D$  instead of the first Fresnel zone for  $x/L = 0.5$ , showing that a LAS is most sensitive to  $D$  sized scales.

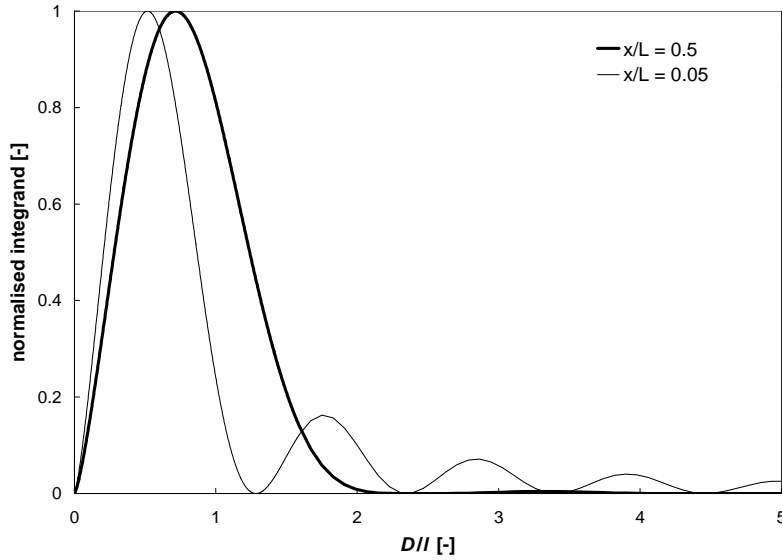


**Figure 14: Values of the integrand (normalized to 1) as a function of the size of the inhomogeneity  $l$ , which is normalized by the aperture diameter  $D$  (for  $x/L = 0.5$  and  $0.05$ ).**

According to Wang et al. (1978) the diameter of the aperture should be sufficiently large in order to avoid saturation. They derived the following criterion

$$\frac{D}{\sqrt{\lambda L}} > 0.98(\sigma_{\chi}^2)^{3/5}. \quad (2.29)$$

By substituting the latter Equation in Equation 2.27 the maximum value for  $C_n^2$  can be derived, which is a function of aperture diameter, the path length and the optical wavelength

$$C_n^2 < 0.93D^{5/3}L^{-8/3}\lambda^{2/6}. \quad (2.30)$$

Based on experimental measurements Ochs and Hill (1982) found that the restriction given by Wang et al. (1978) was too optimistic. They proposed the following criteria

$$\frac{D}{\sqrt{\lambda L}} > 2.7(\sigma_{\chi}^2)^{3/5} \quad (2.31)$$

and thus as maximum  $C_n^2$

$$C_n^2 < 0.18D^{5/3}L^{-8/3}\lambda^{2/6}. \quad (2.32)$$

Their criterion is about 5 times stricter than Wang et al. (1978) proposed. However, it must be noted that Ochs and Hill used dual-aperture tangent detector scintillometers instead of single-aperture detector designs. Frehlich

and Ochs (1990) also studied the saturation effect on optical large aperture scintillometers. They found that for  $\sigma_\chi^2$  values of about 0.03 the large aperture scintillometer underestimated the fluxes in the order of 10% (see Kohsiek et al., 2002). Based on the  $\sigma_\chi^2$  value of 0.03 the following criteria can be derived

$$\frac{D}{\sqrt{\lambda L}} > 5.4(\sigma_\chi^2)^{3/5} \quad (2.33)$$

and

$$C_n^2 < 0.057 D^{5/3} L^{-8/3} \lambda^{2/6}, \quad (2.34)$$

which is about 3 times stricter than Ochs and Hill (1982). Frehlich and Ochs (1990) studied the effect of saturation in strong turbulence by comparing observations with theoretically derived predictions of saturation effects. However, a complete analysis could not be done due to missing inner scale measurements. As Frehlich and Ochs noted, further research is required.

Another advantage of the large aperture scintillometer, besides its saturation resistance, is that the effect of inner scale dependence is small (Wang et al., 1978). In Paragraph 5 it was shown that if the Fresnel size for a point source/detector configuration approaches the size of  $l_o$  inner scale effects could no longer be ignored. This means that an exact shape of the spectrum of refractive index fluctuations ( $\Phi(\kappa)$ ) is required in order to derive  $C_n^2$  from  $\sigma_\chi^2$  measurements. The same applies for large aperture scintillometers, i.e., when the diameter of the aperture becomes too small the scintillometer loses its calibration and becomes dependant on  $l_o$ . Hill and Ochs (1978) found that aperture diameter should be 20 times larger than  $l_o$  to be inner scale independent.

## 8 Related structure parameters

Temperature ( $T$ ), humidity ( $Q$ ) and to a lesser extend pressure ( $P$ ) fluctuations cause fluctuations in the refractive index of air ( $n$ ). By neglecting pressure fluctuations  $C_n^2$  can be related to the structure parameters of temperature ( $C_T^2$ ), humidity ( $C_Q^2$ ) and the covariant term ( $C_{TQ}$ ) as follows (Hill et al., 1980)

$$C_n^2 = \frac{A_T^2}{T^2} C_T^2 + \frac{2A_T A_Q}{TQ} C_{TQ} + \frac{A_Q^2}{Q^2} C_Q^2. \quad (2.35)$$

$A_T$  en  $A_Q$  are functions of the wavelength and the mean values of temperature, humidity and atmospheric pressure (Hill et al., 1980; Andreas, 1989). For visible and near-infrared wavelengths ( $\lambda$  between 0.36-3  $\mu\text{m}$ )  $A_T$  and  $A_Q$  are defined as follows

$$A_T = -m_1(\lambda) \left( \frac{P}{T} \right) - R_v m_2(\lambda) Q, \quad (2.36)$$

$$A_Q = R_v m_2(\lambda) Q, \quad (2.37)$$

where  $R_v$  is the specific gas constant for water vapour ( $461.5 \text{ J K}^{-1} \text{ kg}^{-1}$ ). In case of a near-infrared wavelength of  $940 \text{ nm}$   $m_1 = 0.78 \times 10^{-6} \text{ K Pa}^{-1}$  and  $m_2 = -0.126 \times 10^{-6} \text{ K Pa}^{-1}$ . At radio wavelengths ( $\lambda > 3 \text{ mm}$ )  $A_T$  and  $A_Q$  are slightly different (Kohsiek and Herben, 1983; Andreas, 1989)

$$A_T = - \left( \frac{0.776 \times 10^{-6} P}{T} + \frac{1.723 Q}{T} \right), \quad (2.38)$$

$$A_Q = \left( \frac{1.723 Q}{T} \right). \quad (2.39)$$

In Table 1 typical values for  $A_T$  and  $A_Q$  are given. For a wavelength of  $940 \text{ nm}$  it can be seen that  $A_T \gg A_Q$ . This means that at this wavelength temperature fluctuations are dominant. At radio wavelengths (e.g.  $11 \text{ mm}$ )  $A_Q$  approaches  $A_T$ , i.e., both humidity fluctuations and temperature fluctuations are important. Table 2 shows some values of  $C_n^2$  measured with a near-infrared and radio wave scintillometer and the contributions of  $T$  and  $Q$ .

**Table 1: Typical values for  $A_T$  and  $A_Q$  for 'normal' atmospheric conditions for  $\lambda = 940 \text{ nm}$  and  $\lambda = 11 \text{ mm}$  ( $P = 1 \times 10^5 \text{ Pa}$ ,  $T = 288 \text{ K}$  and  $Q = 0.012 \text{ kg m}^{-3}$ ).**

	$A_T [-]$	$A_Q [-]$
$\lambda = 940 \text{ nm}$	$-0.27 \times 10^{-3}$	$-0.70 \times 10^{-6}$
$\lambda = 11 \text{ mm}$	$-0.34 \times 10^{-3}$	$0.72 \times 10^{-4}$

**Table 2:  $C_n^2$  values measured with a near-infrared and a radio wave scintillometer and contributions of  $C_T^2$ ,  $C_Q^2$  and  $C_{TQ}$  to  $C_n^2$  (Flevoland experiment, 1998)**

	$C_n^2$	$\frac{A_T^2}{T^2} C_T^2$	$2 \frac{A_T A_Q}{T Q} C_{TQ}$	$\frac{A_Q^2}{Q^2} C_Q^2$
$\lambda = 940 \text{ nm}$	$1.22 \times 10^{-14}$	$1.09 \times 10^{-14}$	$1.19 \times 10^{-15}$	$3.89 \times 10^{-17}$
$\lambda = 11 \text{ mm}$	$8.7 \times 10^{-13}$	$1.7 \times 10^{-14}$	$-2.49 \times 10^{-13}$	$1.10 \times 10^{-12}$

The problem is to solve Equation 2.35. Kohsiek (1982a) suggested measuring  $C_n^2$  at three different wavelengths in order to obtain  $C_T^2$ ,  $C_Q^2$  and  $C_{TQ}$ . However, the problem is that there is no wavelength where only humidity fluctuations are dominant. To some degree temperature fluctuations always play a role at most wavelengths (e.g., see Table 2). Kohsiek and Herben (1983) proposed as an alternative to use two wavelengths plus an extra relation between  $T$  and  $Q$  fluctuations instead.

Following the suggestion of Kohsiek and Herben, Andreas (1989) found that a combination of a visible to near-infrared scintillometer and a near-millimetre to radio wave scintillometer, denoted as the ‘two-wavelength method’, is the best option for measuring the fluxes of  $H$  and  $L_vE$ . Both Hill et al. (1988) and Andreas (1989) presented a method to solve  $C_T^2$  and  $C_Q^2$  from  $C_n^2$  values measured at a near-infrared (<sub>nir</sub>) and a radio wavelength (<sub>rw</sub>) thereby assuming  $R_{TQ}\sqrt{C_T^2 C_Q^2} = C_{TQ}$  in order to eliminate  $C_{TQ}$

$$C_Q^2 = \frac{A_{T\_rw}^2 C_{n\_nir}^2 + A_{T\_nir}^2 C_{n\_rw}^2 + 2R_{TQ}\sqrt{C_{n\_rw}^2 C_{n\_nir}^2}}{(\overline{\Gamma T})^2}, \quad (2.40)$$

$$C_T^2 = \frac{A_{Q\_rw}^2 C_{n\_nir}^2 + A_{Q\_nir}^2 C_{n\_rw}^2 + 2R_{TQ}\sqrt{C_{n\_rw}^2 C_{n\_nir}^2}}{(\overline{\Gamma Q})^2} \quad (2.41)$$

with

$$\Gamma = \frac{A_{T\_rw}A_{Q\_nir} - A_{T\_nir}A_{Q\_rw}}{TQ}. \quad (2.42)$$

$R_{TQ}$  is the correlation coefficient between the temperature and the absolute humidity within the inertial sub range. Because in most cases  $C_{TQ}$  is not measured directly, it is customary to assume that  $R_{TQ}$  is  $\pm 1$  in order to estimate  $C_{TQ}$  from  $C_T$  and  $C_Q$ .

In case  $C_n^2$  is measured at only one wavelength Wesely (1976a) showed that at visible to near-infrared wavelengths Equation 2.35 can be rewritten as follows

$$C_n^2 = \frac{A_T^2}{T^2} C_T^2 \left( 1 + R_{Tq} \frac{A_q T C_Q}{A_T Q C_T} \right)^2. \quad (2.43)$$

First, it is assumed that  $R_{TQ}$  equals  $\pm 1$  to get an estimate  $C_{TQ}$ . Second, the Bowen ratio is expressed as

$$\beta = \frac{H}{L_v E} = \frac{\rho c_p \overline{w' T'}}{L_v \overline{w' Q'}} = \frac{\rho c_p C_T}{L_v C_Q}, \quad (2.44)$$

which is used to replace ( $C_T / C_Q$ ). Kohsiek (1982b) experimentally showed that  $\beta$  could be derived from  $C_T$  and  $C_Q$  measurements. Finally, this leads to the following very practical Equation (using  $\rho = 1.2 \text{ kg m}^{-3}$ ,  $c_p = 1005 \text{ J kg}^{-1} \text{ K}^{-1}$  and  $L_v = 2.45 \times 10^6 \text{ J kg}^{-1}$ )

$$C_n^2 \approx \frac{A_T^2}{T^2} C_T^2 \left( 1 + \frac{0.03}{\beta} \right)^2, \quad (2.45)$$

for deriving  $C_T^2$  from  $C_n^2$  measurements obtained with a visible to near-infrared scintillometer.

## 9 Monin-Obukhov Similarity Theory

In the lowest part ( $\approx 10\%$ ) of the planetary boundary layer (PBL), the surface layer (SL), it is considered that the vertical fluxes of momentum and conservative scalars are nearly constant with height. Within the SL the Monin-Obukhov similarity theory (MOST) makes it possible to link the structure parameter of temperature ( $C_T^2$ ) and humidity ( $C_Q^2$ ) with the surface fluxes  $H$  and  $L_v E$ . Assuming stationary conditions and a horizontal homogeneous surface MOST describes this relationship as follows

$$\frac{C_T^2 (z-d)^{2/3}}{T_*^2} = \frac{C_Q^2 (z-d)^{2/3}}{Q_*^2} f\left(\frac{z-d}{L_{Ob}}\right), \quad (2.46)$$

with  $z$  is the height of the scintillometer above the surface,  $d$  the displacement and  $L_{Ob}$  the Obukhov length

$$L_{Ob} = \frac{u_*^2 T}{g k_v T_*}, \quad (2.47)$$

where  $k_v$  the von Kármán constant. The temperature scale  $T_*$ , the friction velocity  $u_*$  and the absolute humidity scale  $Q_*$ , are defined as follows

$$T_* = \frac{-H}{\rho c_p u_*}, \quad (2.48)$$

$$u_* = \sqrt{\frac{\tau}{\rho}}, \quad (2.49)$$

$$Q_* = \frac{-E}{u_*}. \quad (2.50)$$

Wyngaard et al. (1971) proposed the first expression for  $f$  between  $C_T^2$  and  $H$ , that was based on in-situ measurements done during the Kansas 1968 experiment

$$f\left(\frac{z-d}{L_{Ob}}\right) = c_{T1} \left(1 - c_{T2} \frac{z-d}{L_{Ob}}\right)^{-2/3} \quad \text{for} \quad \left(\frac{z-d}{L_{Ob}}\right) < 0, \quad (2.51)$$

with  $c_{T1} = 4.9$  and  $c_{T2} = 7$ . This expression is only valid for unstable atmospheric conditions. Alternative expressions have been proposed (Wesely, 1976b; Andreas, 1988; Thiermann and Grassl, 1992; Hill et al., 1992a; De Bruin et al., 1993) for both unstable (some examples are depicted in Figure 15) and stable conditions. Most proposed expressions are based on in-situ eddy covariance observations of the Kansas experiment (Wyngaard et al., 1971; Andreas, 1988). Interesting to note is that it is not known how well the eddy covariance derived fluxes did close the energy balance during these experiments (Kohsiek et al., 2002), which questions the validity of  $f$ .

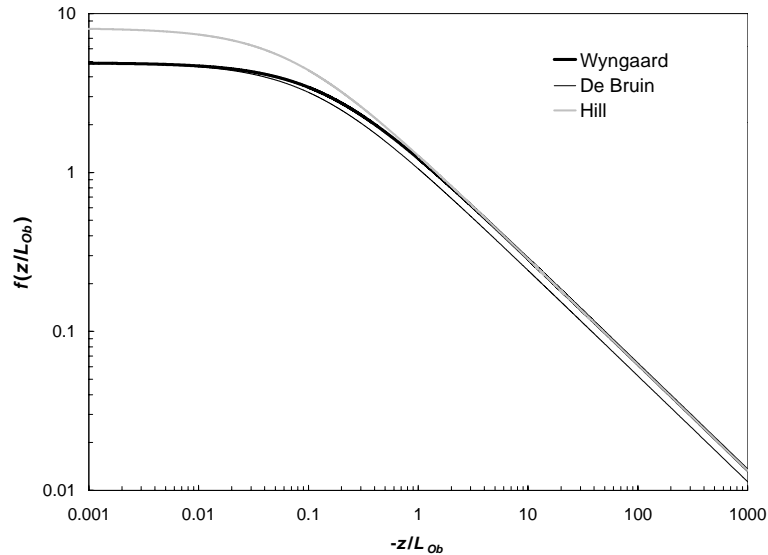


**Figure 15: Stability functions proposed by Wyngaard, De Bruin and Hill for unstable conditions ( $z/L_{Ob} < 0$ ).**

In order to solve  $H$  the friction velocity is required. The friction velocity can be determined using different techniques. First, measure the inner scale  $l_o$  using a small aperture scintillometer (see e.g., Hill et al., 1992a; Thiermann, 1992; Thiermann and Grassl, 1992). Once the inner scale is known  $u_*$  and the fluxes can be derived

iteratively. Second, an eddy covariance system can be used to measure the friction velocity ( $u_* = \sqrt{-\overline{u'w'}}$ ). Third,  $u_*$  can be derived by applying the  $C_T^2$  - profile method proposed by Hill et al. (1992b) thereby using two large aperture scintillometers installed at two different heights. Finally, the friction velocity can be obtained from wind speed data ( $u$ ) and an estimate of the surface roughness ( $z_0$ )

$$u_* = \frac{k_v u}{\ln\left(\frac{z_u - d}{z_0}\right) - \Psi_m\left(\frac{z - d}{L_{Ob}}\right) + \Psi_m\left(\frac{z_0}{L_{Ob}}\right)}. \quad (2.52)$$

$\Psi_m$  is the well-known Businger-Dyer expression. The main advantage of the first and third method is that path averaged values for  $u_*$  can be derived. The second and latter methods are ‘traditional’ point techniques for estimating  $u_*$ . For these cases one can question their representativeness over non-homogeneous areas.

For very unstable atmospheric conditions ( $-\frac{z-d}{L_{Ob}} > 1$ ) the following simple expression for the sensible heat flux can be derived

$$H = \rho c_p b (z - d) \left(\frac{g}{T}\right)^{1/2} (C_T^2)^{3/4}, \quad (2.53)$$

where  $b = \sqrt{\left(\frac{1}{c_{T1}}\right)^{3/2} k_v c_{T2}}$  varies between 0.48 and 0.57 (Kohsiek, 1982b; De Bruin et al., 1995). This expression is also known as the free convection limit and provides a simple method to determine  $H$  directly from  $C_T^2$  without knowing  $u_*$ . In practical applications the free convection approach can provide accurate fluxes when the scintillometer is installed relatively high above the surface ( $\approx 10$  m). Despite its simplicity it must be noted that the measurement height of the scintillometer should be measured accurately because  $H$  is linearly related to the measurement height ( $z-d$ ) (see e.g., Hartogensis et al., 2002b). In non-flat areas this can be complicated.

## 10 Summary

In the preceding Paragraphs the basics of the scintillation method is explained. Based on the Rytov method it is now possible to describe the propagation of EM radiation in a turbulent medium. This means that we can link the propagation statistics of EM radiation (i.e. the Rytov variance  $\sigma_x^2$ ) with the characteristics of the atmosphere ( $C_n^2$ ) using a small aperture or point source/detector scintillometer (further denoted as SAS). A scintillometer is considered a SAS when its diameter is smaller than first Fresnel zone ( $F$ ). However the proportionality between

$\sigma_\chi^2$  and  $C_n^2$  is only valid when  $\sigma_\chi^2$  remains smaller than 0.3. Above this limit the signal becomes saturated. This means that for near infrared to visible wavelengths the optical path is restricted to short distances of approximately 250 m. In the radio wavelength region saturation is less likely and the distance can be several kilometres. Turbulent scales in the order of the first Fresnel zone ( $F$ ) primarily cause the scintillations observed by a SAS. Depending on the operational wavelength of the light source  $F$  varies between several millimetres (near infrared region) to a few meters (radio wave region). A near-infrared SAS is therefore very sensitive to inner scale effects. Outer scale effects are relevant in the propagation statistics of radio waves meaning that non-isotropic conditions can distort the measurements. Another problem is that at radio wavelengths also absorption fluctuations by water molecules influence the intensity statistics.

The large aperture scintillometer (LAS) and the extended XLAS, which operate in the near infrared region, are designed to overcome the saturation effect of the near-infrared SAS. Due to the increased aperture small-scale structures are filtered out, which lead to a reduction of the amount of scintillations. As a result the LAS can operate over longer distances, i.e., the proportionality between  $\sigma_\chi^2$  and  $C_n^2$  remains valid under strong turbulent conditions. Although the LAS and XLAS also have a saturation maximum, it has not been thoroughly investigated. Another advantage of the LAS is that the instrument is most sensitive to eddy sizes in the order of its diameter (LAS,  $D = 0.15$  m; XLAS,  $D = 0.31$  m), which lie far from the inner scale and outer scale. As a result the LAS is less sensitive to inner scale and outer scale effects. In Table 3 an overview is given of different, widely used, scintillometer types; the near-infrared small aperture scintillometer (SAS), the near-infrared large aperture scintillometers (LAS and XLAS) and the radio wave small aperture scintillometer (RW-SAS); their operational regimes, characteristic length scales and sensitivities. The LAS, XLAS and SA-RWS have the potential to obtain surface fluxes over spatial scales of several kilometres (see Chapter 3 and 4).

**Table 3: Overview of different scintillometer types: the near infrared small aperture (SAS), the large aperture scintillometer (LAS and XLAS) and the small aperture radio wave scintillometer (SA-RWS).**

	<i>SAS</i>	<i>LAS</i>	<i>XLAS</i>	<i>SA-RWS</i>
$\lambda$	670 nm	940 nm	940 nm	11 mm
$L$	20 – 250 m	500 – 5000 m	1 – 10 km	1 – 10 km
$F$	$\approx 0.01$ m	$\approx 0.05$ m	$\approx 0.08$ m	$\approx 5$ m
$D$	$\approx 0.002$ m	0.15 m	0.31 m	0.6 m
Most effective eddy	$\approx F$	$\approx D$	$\approx D$	$\approx F$
Restrictions of:				
$\sigma_\chi^2$ (saturation)	$< 0.3$	$\frac{D}{\sqrt{\lambda L}} > 2.7(\sigma_\chi^2)^{3/5}$	$\frac{D}{\sqrt{\lambda L}} > 2.7(\sigma_\chi^2)^{3/5}$	$< 0.3$
$D$ ('inner scale dependence')	-	$D \gg 20l_o$	$D \gg 20l_o$	-
$D$ ('aperture averaging')	-	$D > 2F$	$D > 2F$	-
$F, D$	$l_o \approx F \ll L_o$	$l_o \ll F \ll D < L_o$	$l_o \ll F \ll D < L_o$	$l_o \ll F \ll L_o$

Once  $C_n^2$  is known,  $C_T^2$  and/or  $C_Q^2$  can be derived depending on the scintillometer configuration (a near-infrared SAS, LAS or a combined LAS - SA-RWS configuration). The final step is to relate  $C_T^2$  and/or  $C_Q^2$  to the surface fluxes of sensible and latent heat applying MOST. The latter step is most sensitive to distortions, especially when  $C_n^2$  is obtained over long path lengths of several kilometres since MOST requires stationary and homogeneous surface conditions. This issue will be discussed in the next chapters.

Based on the restrictions of e.g., the LAS given in Table 3, the operational regime of the LAS can be derived, which is shown in Figure 16. The minimal height of the LAS is estimated for 6 different surface characteristics ( $H = 100 \text{ W m}^{-2}$  to  $600 \text{ W m}^{-2}$ ) and path lengths using the proposed saturation regime of Ochs and Hill (1982) and applying the free convection approach. The area below the 6 curves represents the area where saturation occurs. It can be seen that for a constant height and path length over wet areas the LAS can be installed at lower heights than over dry areas. The maximum path length of a LAS is approximately 5 km in order to satisfy the criterion that the diameter must be larger than two times the Fresnel zone  $F$ . The minimum distance of the LAS is approximately 500 m and depends solely on the signal-to-noise characteristics of its electronics. It has been shown in Paragraph 9 that in the surface layer (10% of the boundary layer height,  $h$  or  $z_i$ ), when  $-\frac{z-d}{L_{Ob}} > 1$  the

local free convection approach can be applied, and  $u_*$  no longer is an important MOST variable. Above the surface layer, inside the mixed layer the structure functions can be scaled as a function of large-scale structures in the order of the boundary layer height ( $h$  or  $z_i$ ) instead of MOST. Experimental data have shown (see e.g., Wyngaard and LeMone, 1980; Kohsiek, 1988) that this mixed-layer-scaling holds only in the lower part of the convectively driven boundary layer ( $0.2z_i \sim 0.3z_i$ ), and thus limits the installation-height of the scintillometer.

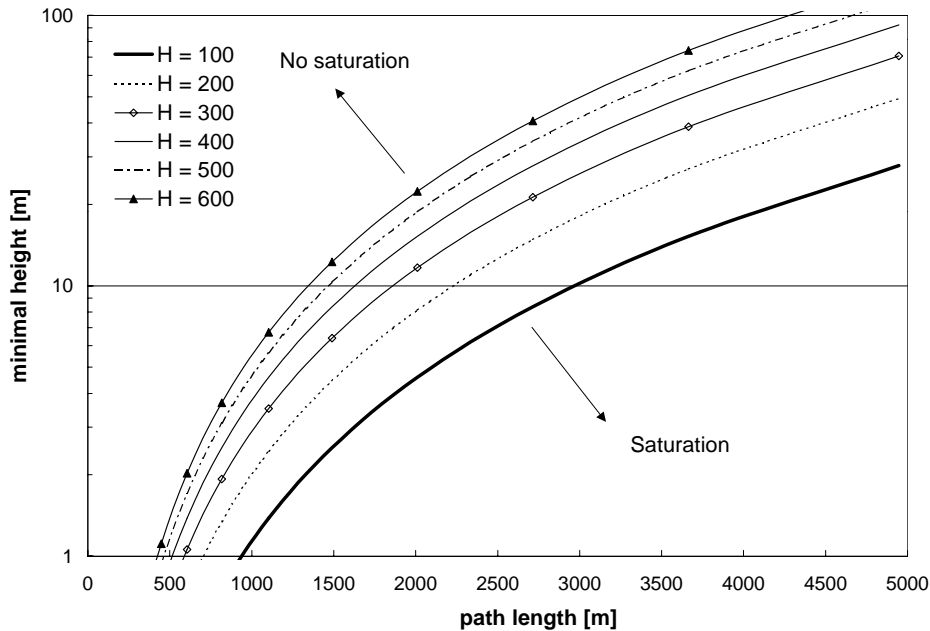


Figure 16: Operational regimes of the LAS.

## References

- Andreas, E. L.: 1988, 'Estimating  $C_n^2$  over Snow and Sea Ice from Meteorological Data', *J. Opt. Soc. Am.* **5**, 481-495.
- Andreas, E. L.: 1989, 'Two-Wavelength Method of Measuring Path-Averaged Turbulent Surface Heat Fluxes', *J. Atm. Ocean. Tech.* **6**, 280-292.
- Andreas, E. L.: 1990, *Selected Papers on Turbulence in a Refractive Medium*, SPIE Milestone Series 25, SPIE - The International Society for Optical Engineering, Bellingham, 693 pp.
- Andrews, L.C.: 1992, 'An Analytical Model for the Refractive Index Power Spectrum and its Application to Optical Scintillations in the Atmosphere', *J. Mod. Opt.* **39**, 1849-1853.
- De Bruin, H. A. R., Kohsiek, W. and Van den Hurk, B. J. J. M.: 1993, 'A Verification of Some Methods to Determine the Fluxes of Momentum, Sensible Heat and Water Vapour using Standard Deviation and Structure Parameter of Scalar Meteorological Quantities', *Boundary-Layer Meteorol.* **63**, 231-257.
- De Bruin, H. A. R. and Meijninger, W. M. L.: 2002, 'Displaced-Beam Small Aperture Scintillometer Test Part I: The WINTeX Data-Set', *Boundary-Layer Meteorol.* In press.
- Churnside, J. H.: 1990, 'A Spectrum of Refractive Turbulence in the Turbulent Atmosphere', *J. Mod. Optics* **37**, 13-16.
- Clifford, S. F., Ochs, G. R. and Lawrence, R.S.: 1974, 'Saturation of Optical Scintillation by Strong Turbulence', *J. Opt. Soc. Am.* **64**, 148-154.
- Frehlich, R. G. and Ochs, G. R.: 1990, 'Effects of Saturation on the Optical Scintillometer', *Applied Optics* **29**, 548-553.
- Garrat, J. R.: 1992, *The Atmospheric Boundary Layer*, University Press, Cambridge, 316 pp.
- Hartogensis, O .K., De Bruin, H. A. R. and Van de Wiel, B. J. H.: 2002a, 'Displaced-Beam Small Aperture Scintillometer test Part II: CASES-99 stable boundary layer experiment', *Boundary-Layer Meteorol.* In press.
- Hartogensis, O. K., Watts, C. J., Rodriguez, J. C. and De Bruin, H. A. R.: 2002b, 'Derivation of an Effective Height for Scintillometers: La Poza Experiment in Northwest Mexico', submitted to *Hydrometeorology*.

Hill, R. J. and Ochs, G.R.: 1978, 'Fine Calibration of Large-Aperture Optical Scintillometers and an Optical Estimate of Inner Scale of Turbulence', *Applied Optics* **17**, 3608-3612.

Hill, R. J., Clifford, S. F. and Lawrence, R. S.: 1980, 'Refractive-Index and Absorption Fluctuations in the Infrared Caused by Temperature, Humidity and Pressure Fluctuations', *J. Opt. Soc. Am.* **70**, 1192-1205.

Hill, R. J., Bohlander, R. A., Clifford, S.F., McMillan, R. W., Priestley, J. T. and Schoenfeld, W. P.: 1988, 'Turbulence-Induced Millimetre-Wave Scintillation Compared with Micrometeorological Measurements', *IEEE Trans. Geosci. Remote Sensing* **26**, 330-342.

Hill, R. J., Ochs, G. R. and Wilson, J. J.: 1992a, 'Measuring Surface-Layer Fluxes of Heat and Momentum Using Optical Scintillation', *Boundary-Layer Meteorol.* **58**, 391-408.

Hill, R. J., Ochs, G. R. and Wilson, J. J.: 1992b, 'Surface-Layer Fluxes Measured Using the  $C_T^2$  - Profile Method', *J. Atmos. Ocean. Tech.* **9**, 526-537.

Kohsiek, W., 1982a, *Optical and In-Situ Measuring of Structure Parameters Relevant to Temperature and Humidity, and Their Application to the Measuring of Sensible and Latent Heat Flux*, NOAA Tech. Memor. ERL WPL-96, NOAA Environmental Research Laboratories, Boulder, CO, USA, 64 pp.

Kohsiek, W., 1982b, 'Measuring  $C_T^2$ ,  $C_q^2$  and  $C_{Tq}$  in the Unstable Surface Layer, and Relations to the Vertical Fluxes of Heat and Moisture', *Boundary-Layer Meteorol.* **24**, 89-107.

Kohsiek, W. and Herben, M. H. A. J.: 1983, 'Evaporation Derived from Optical and Radio Wave Scintillation', *Appl. Opt.* **22**, 2566-2569.

Kohsiek, W.: 1984, 'Inertial Subrange Correlation between Temperature and Humidity Fluctuations in the Unstable Surface Layer above Vegetated Terrains', *Boundary-Layer Meteorol.* **29**, 211-224.

Kohsiek, W.: 1988, 'Observation of the Structure Parameters  $C_T^2$ ,  $C_{TQ}$  and  $C_Q^2$  in the Mixed Layer over Land', *Appl. Opt.* **27**, 2236-2240.

Kohsiek, W., Meijninger, W. M. L., Moene, A. F., Heusinkveld, B. G., Hartogensis, O. K., Hillen, W. C. A. M. and De Bruin, H. A. R.: 2002, 'An Extra Large Aperture Scintillometer (XLAS) with a 9.8 km Path Length', *Boundary-Layer Meteorol.* In press

Lawrence, R. S. and Strohbehn, J. W.: 1970, 'A Survey of Clear-Air Propagation Effects Relevant to Optical Communications', *Proceedings of the IEEE* **58**, 1523-1545.

Moene, A.F.: 2001, 'A Review of the Relationships Describing the Signal of a Large Aperture Scintillometer', internal report.

Ochs, G. R. and Hill, R. J.: 1982, *A Study of Factors Influencing the Calibration of Optical  $C_n^2$  Meters*, NOAA Tech. Memor. ERL WPL-106, NOAA Environmental Research Laboratories, Boulder, CO, USA, 24 pp.

Tatarskii, V. I.: 1961, *Wave Propagation in a Turbulent Medium*, Translated from Russian by R. S. Silverman, McGraw-Hill, New York, USA, 285 pp.

Tatarskii, V.I.: 1971, *The Effect of the Turbulent Atmosphere on Wave Propagation*, translated from Russian by Israel Program for Scientific Translation, Springfield, Va, USA, 472 pp.

Thiermann, V.: 1992, 'A Displaced Beam Scintillometer for Line-Averaged Measurements of Surface Layer Turbulence', *10th Symposium on Turbulence and Diffusion*, Portland Oregon, September 29 - October 2, 1992, American Meteorological Society, Boston, MA, pp. 244-247

Thiermann, V. and Grassl, H.: 1992, 'The Measurement of Turbulent Surface Layer Fluxes By Use of Bichromatic Scintillation', *Boundary-Layer Meteorol.* **58**, 367-389.

Wang, T. I., Ochs, G. R., and Clifford, S. F.: 1978, 'A Saturation-Resistant Optical Scintillometer to Measure  $C_n^2$ ', *J. Opt. Soc. Am.* **69**, 334-338.

Wesely, M. L.: 1976a, 'The Combined Effect of Temperature and Humidity on the Refractive Index', *J. Appl. Meteorol.* **15**, 43-49.

Wesely, M. L.: 1976b, 'A Comparison of Two Optical Methods for Measuring Line Averages of Thermal Exchange Above Warm Water Surfaces', *J. Appl. Meteorol.* **15**, 1177-1188.

Wyngaard, J. C., Izumi, Y. and Collins Jr., S. A.: 1971, 'Behaviour of the Refractive-Index-Structure Parameter Near the Ground', *J. Opt. Soc. Am.* **61**, 1646-1650.

Wyngaard, J. C. and LeMone, M. A.: 1980, 'Behavior of the Refractive Index Structure Parameter in the Entraining Convective Boundary Layer', *J. Atm. Sciences* **37**, 1573-1585.